Hindawi
Advances in Materials Science and Engineering
Volume 2018, Article ID 6767245, 8 pages
https://doi.org/10.1155/2018/6767245

Research Article

Surface Characterization of Three-Layer Organic Coating Applied on AISI 4130 Steel

Ane C. Rovani, Fernanda Kouketsu, Carlos H. da Silva, and Giuseppe Pintaude

Academic Department of Mechanics (DAMEC), Federal University of Technology-Paraná (UTFPR), Rua Deputado Heitor Alencar Furtado 5000–Ecoville, 81280-340 Curitiba, PR, Brazil

Correspondence should be addressed to Giuseppe Pintaude; giuseppepintaude@gmail.com

Received 14 December 2017; Revised 14 February 2018; Accepted 22 February 2018; Published 29 March 2018

Academic Editor: Yuanshi Li

Resin-bonded molybdenum disulfide (MoS_2) is widely applied as a solid lubricant. However, multiple coatings are usually required to meet other requirements in mechanical systems. In this study, a quenched and tempered AISI 4130 steel was used as the substrate, being shot blasted. Furthermore, three layers were successively deposited: a zinc phosphate layer, a phenolic resin (basecoat), and a topcoat based on MoS_2. The thicknesses of different layers were obtained by scanning electron microscope and by the ball-cratering method. 3D surface roughness parameters were determined for each step of manufacturing, following three approaches: average values, isotropy level, and distribution of heights. The ball-cratering method was successfully applied for determining the thickness of the zinc phosphate but presented a relative deviation for the others layers. The phosphating step was decisive for the final surface topography of resin-bonded coating in terms of distribution of heights. On the other hand, the isotropy level imposed by the shot blasting of steel was practically unaltered by all manufacturing processes.

1. Introduction

Molybdenum disulfide (MoS_2) is a well-known solid lubricant, and its tribological properties are associated with its lamellar morphology, which facilitates the sliding among surfaces in contact [1–3].

Different processes have been applied to obtain coatings based on MoS_2. Amongst them are burnishing, sputtering, and spraying [4]. The last one is used to produce resin-bonded MoS_2, which is perhaps the most common product for achieving a self-lubricating film on metal surfaces.

However, to meet the requirements needed in offshore devices exposed to a saline environment, the protective coating should perform multiple functions [5]. The use of a solid lubricant as a filler cannot be enough to guarantee all required functions, especially the corrosion resistance. To check the performance, several tests and analysis may be done, such as those described by Momber et al. [6] for a dual-layer organic coating. Most of these characterizations are related to the surface integrity, which in turn are dependent on the surface roughness.

Some investigations deserved attention only for a limited characterization of surface roughness, although it plays a key role in the manufacturing of coatings. Lin and Yan Guu [7] evaluated only the bidimensional average roughness Ra for three primary processes (shot blasting, phosphatizing, and salt-bath soft nitriding) previously applied onto a ground surface of steel before the final treatment to obtain a topcoat of MoS_2. In the same way, Roberts and Williams [8] investigated the effect of the surface roughness on the tribological performance of sputtered MoS_2 films, but their approach was again limited to two-dimensional characterization and restricted to the average roughness.

In this context, this manuscript aims to bring a complete description of surface characterization of multiple-layered coatings, especially for the changes in surface roughness at each step of manufacturing, using a 3D approach to measurement. In addition, the usefulness of the use of the

ball-cratering method for a three-layer organic coating is described.

2. Materials and Methods

2.1. Materials. A quenched and tempered steel (AISI 4130) for 233 HV was used as the substrate. It was subject to the shot-blasting process for cleaning purposes, performed with brown aluminum oxide (Al_2O_3) particles of 35–70 mesh (212–600 μm).

The manufacturing of a resin-bonded MoS_2 constituted three more steps. Firstly, a layer of zinc phosphate was deposited onto the substrate, composed mainly by ZnP_4 and ZnO, as presented elsewhere [9]. The zinc phosphate layer was prepared in a bath. Furthermore, an epoxy phenolic resin was added, called here as the basecoat (primer). With this layer, besides the improvement of corrosion resistance, it is expected a correction on the waviness caused by the shot-blasting process previously applied on the substrate. Finally, a thermostable phenolic resin based on MoS_2 composition (called as the topcoat) was added. The application method used for both layers (top- and basecoat) was the spray. Then, the curing process was carried out at 80–90°C. The topcoat contains a significant amount of Sb_2O_3 (diantimony trioxide), as already described in [9]. This oxide can act positively in a tribosystem, acting against tribo-oxidation and providing a mechanical support tribofilm for MoS_2 [10].

2.2. Characterization. Coatings were characterized considering their morphology and surface topography. Cross-sectional and superficial views were used for that. Both sections were prepared to reach a surface roughness equivalent to that obtained in a polishing process, through metallographic techniques.

The morphology and thickness of coatings were evaluated using scanning electron microscope (SEM). The top section was preferred to describe the morphology, while the measurement of thickness was made at the cross-sectional ones. Regarding the chemical composition, the energy dispersive X-ray spectroscopy (EDS) coupled to an SEM was used for this purpose.

Additionally, the thickness was evaluated with a ball-cratering method. The Calotest® is an equipment used to measure the coating thickness between 0.1 and 50 μm. The main reason for its use is to provide faster results, without a need to prepare a metallographic section of the coating. The dimensions of the crater, a depression with the shape of a spherical cap, can be obtained by using optical microscopy (OM) or SEM.

With the dimensions of the crater, the thickness of the coating (t) can be calculated, following (1), according to ISO-26423 : 2009 [11]. For multiple layers, Figure 1 shows a schematic representation used here for the resin-bonded MoS_2.

$$t = \frac{X \cdot Y}{\phi_{\text{ball}}}, \tag{1}$$

where X and Y are the depressions of the projected surfaces of the coating and substrate sections and ϕ_{ball} is the diameter of the ball.

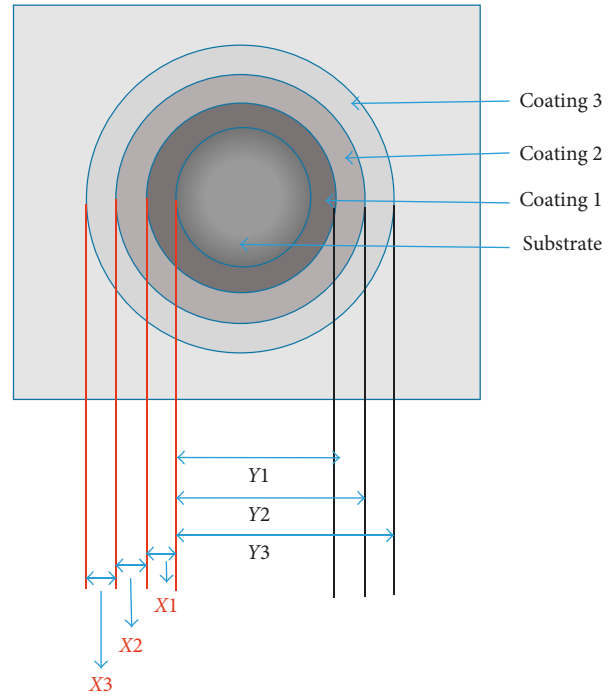

Figure 1: Schematic representation of ISO-26423:2009 to thickness determination for coating with multiple layers.

Table 1: Parameters used in the ball-cratering method.

Parameters	Conditions
Rotation (rpm)	1000
Angle (°)	38
Rotation sense (CW or CCW)	Clockwise (CW)
Tangential speed (m/s)	1.57
Ball diameter (mm)	30
Load (N)	0.66
Abrasive slurry	Particles: 0.05–0.1 μm/water

Table 1 shows the parameters selected for the determination of the thickness of coating in the ball-cratering method. We have opted by using a standard solution supplied by CSM Instruments in the smallest available size range (0.05–0.1 μm), following the recommendation made in [12]. In addition, a dilution during the tests was performed using distilled water, dripping water every 5 minutes on the ball surface.

Another important aspect done for the ball-cratering method here was the preconditioning of the ball. This variable was investigated by Allsopp et al. [13], and they verified a difficulty in the use of a polished new ball for relatively soft specimens, which would be our case. To avoid this situation, at every hour, the ball was exposed to a manual agitation in a recipient full of a dry standard sand (A100) for 3 to 5 minutes. This operation led the ball surface roughness Ra to values of 0.20 ± 0.06 μm, guaranteeing a better particle entrainment during the tests [13].

The technique of coherence correlation interferometry (CCI) was employed to obtain 3D asperity information of each step of deposition. This equipment operates with a vertical

resolution of 0.01 nm and 1.63 μm for the lateral one. Four 3D parameters were selected for further analysis: the height parameter Sq (*root-mean-square*), the height distribution parameters Ssk (*skewness*) and Sku (*kurtosis*), besides the spatial parameter Str (*texture aspect ratio*).

The sampling area used for the 3D characterization was 0.83 mm^2, obtained from a combination between the lens and the resolution. The magnification of 20 times and 512 pixels of the resolution were used to achieve that purpose. Each average value of roughness parameters corresponds to a series of 6 measurements.

3. Results and Discussions

3.1. Overview of Deposited Layers and Thickness Determination. Figure 2(a) shows the transversal section obtained by SEM, and Figure 2(b) shows the crater image obtained by the ball-cratering method to the same studied coating. Three layers were observed in both Figures 2(a) and 2(b). The layer close to the substrate, zinc phosphate, is considered essential for marine environments, promoting a barrier against the corrosion and providing a good adhesion to backing coating together with mechanical anchoring [14]. Furthermore, a basecoat with approximately 15 μm was added, and finally, the topcoat based on the MoS_2 was deposited.

Measured values of thickness are presented in Table 2. As the ball-cratering method is usually applied for hard coatings [15], we separate a single layer of zinc phosphate to test the adequacy of the method when applied to a soft coating (Figure 3). The thickness values determined for this coating using SEM and those observed through the ball-cratering method were the same.

The found values of the zinc phosphate layers presented in Table 2 showed the efficiency of the ball-cratering method to determine their thickness, as no difference between the measurements made in SEM and the ball-cratering method was detected.

On the other hand, when the thickness of multiple layers is evaluated using the same parameters, a difference between SEM and the ball-cratering method appeared. The problem was clearly associated with the deformation left by a layer over the successive ones. For the topcoat (MoS_2) and for the basecoat (primer resin), the difference was about 37% between methods. When there is more than one coating on the same sample, it is important to note that the measurement of the thickness of the outermost coating is influenced by the measurement of the innermost one, in a successive way. Figure 1 shows clearly that the values of the first coating lead to the determination of the second one and so on. However, it is remarkable that the values of the same order of magnitude use different methods for determining the thickness, showing the adequacy of selected parameters for soft coatings in the ball-cratering method.

For the authors' knowledge, no-one investigation made use of Calotest for phenolic coatings higher than 10 μm thick. Rivero et al. [16] used this technique for measuring the thickness of furan and phenolic coatings but is limited to <3 μm. It is remarkable that the difference of rotation speed used in their investigation (2500 rpm) was much higher than that used here. Besides this variable, we used the conditioning of the ball before tests and an abrasive suspension with smaller particle size.

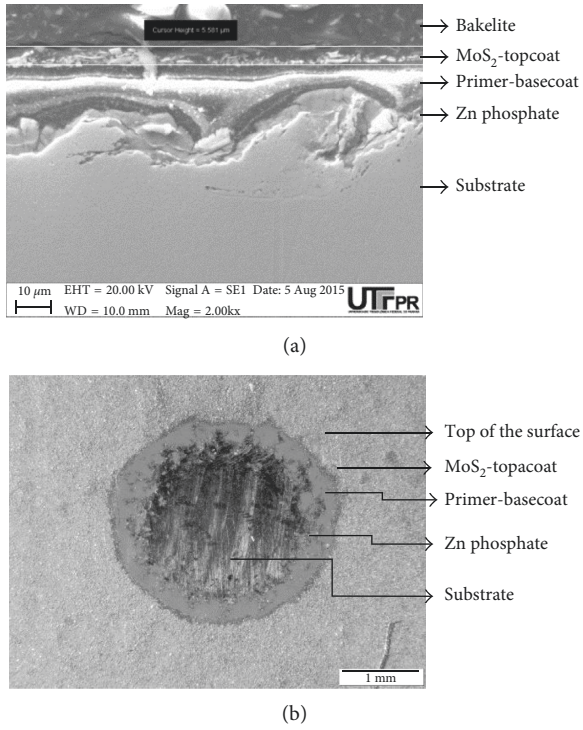

Figure 2: (a) SEM image of cross-sectional areas of the MoS_2 coating system and (b) the surface after the ball-cratering method.

Table 2: Thickness values (μm) obtained in SEM (transversal section) and the ball-cratering method and the respective differences (%) between them.

Coating	SEM	Ball-cratering method	Difference (%)
Zn phosphate (single layer)	11 ± 5	11 ± 3	0
MoS_2 (topcoat)	4.4 ± 0.8	7 ± 2	37.1
Primer (basecoat)	11 ± 1	19 ± 3	36.8
Zn phosphate	8 ± 3	8 ± 2	0

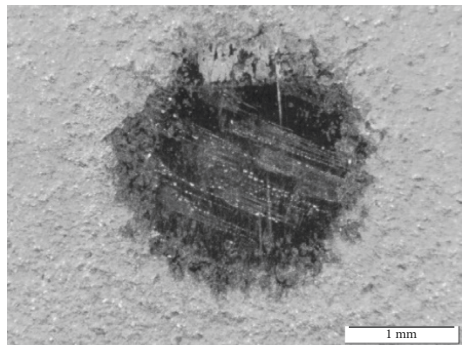

Figure 3: Surface of a single zinc phosphate coating after the ball-cratering method.

3.2. Surface Changes. Towards this more general view of the system, the surface changes caused by each of the processing steps can be described in detail, especially by means of 3D roughness parameters. For the first step of manufacturing, the shot blasting of the steel substrate, it is expected a Gaussian distribution of heights and a highly isotropic surface [17]. This expectation can be confirmed looking at the histogram of height frequencies and the polar graph of texture directions presented in Figure 4, along with the average value of 0.77 ± 0.05 for the Str parameter. Values typically higher than 0.3 for Str mean a high isotropy of surfaces [17], which is the case of this surface.

Lin and Yan Guu [7] identified only a slight increase in the surface roughness Ra when the shot-blasting process was applied onto a ground surface of the steel. They could have given more attention for that point, once the use of shot blasting as the previous treatment for a MoS_2 deposition resulted in the lowest friction coefficient in a ball-on-disk testing apparatus, comparing it with other surface treatments (phosphatizing and salt-bath soft nitriding).

The further step of manufacturing was a deposition of a zinc phosphate layer. Figure 5 reveals a structure in the form of needles for the zinc phosphate layer [18, 19]. Besides, some regions are uncovered revealed by EDS analysis. These discontinuities can be associated with the cleaning process of the substrate, influencing the nucleation and formation of zinc phosphate at the surface [20], and their amount can be responsible for a relatively low performance of this coating against corrosion [19].

Figure 6 shows the 3D surface images of the blasted surface (Figure 6(a)) and zinc phosphate (Figure 6(b)), where it is possible to observe some difference in topography caused by the Zn phosphate deposition.

The deposition of zinc phosphate becomes the surface predominant in peaks, instead of the slight prevalence of valleys as observed for the shot-blasted surface. This surface roughness alteration is the most significant one observed in this investigation.

Following Zhang and Kapoor [21], the initial surface roughness plays a decisive role in the surface texture of a phosphate surface. The main reason for that is that the concentration of solution surrounding peaks is always stronger than that at valleys. Therefore, as the initial difference between peaks and valleys is higher, that is, the higher would be the average roughness, there is a tendency that the phosphating process increases the average roughness itself.

Although the investigation of Zhang and Kapoor made use of a 3D approach of surface texture, they used a stylus profilometer for measuring the surface roughness, which means that the current investigation helps to corroborate its results using another technique (interferometry) and even another approach in terms of surface parameters. For this, the comparison between the Sdq parameter (*root-mean-square slope*) is useful. This parameter was altered from 1.12 to 6.12 as an effect of the phosphating, a much higher increase than that observed for Sq. The change in Sdq means that the phosphating was able to sharpen the asperities, a clear effect of the greater reaction occurred at the peaks.

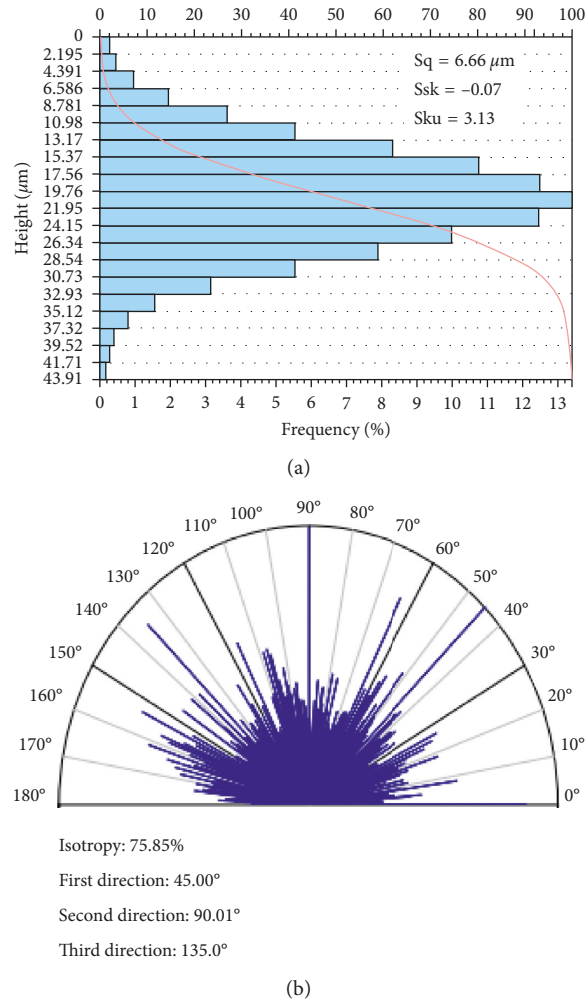

Figure 4: (a) Histogram of height distribution of a representative shot-blasting steel surface and (b) the polar graph with texture directions.

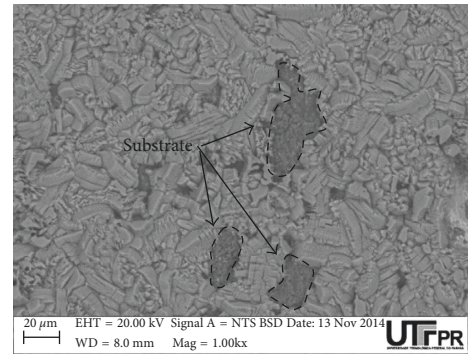

Figure 5: Top surface of the zinc phosphate layer on shot-blasted steel.

An additional layer of phenolic resin was added after the zinc phosphate deposition. This layer is red (Figure 7), being the color easily revealed after a single-point scratch.

Figure 8 shows the SEM image of the basecoat surface, where the secondary electron image (Figure 8(a)) helps to

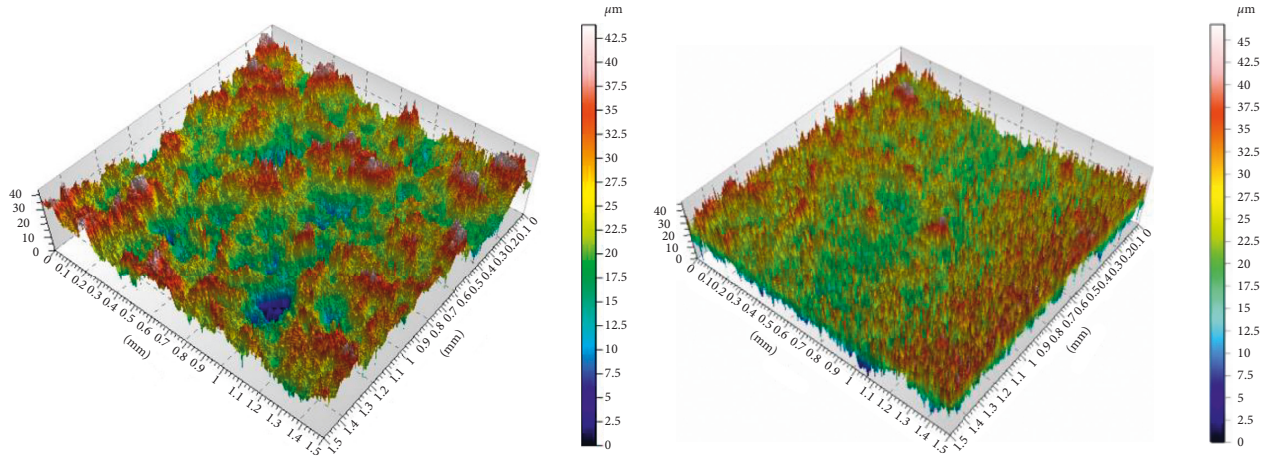

Figure 6: 3D surface images of the (a) shot-blasted surface and (b) zinc phosphate layer.

identify the topography and the backscattered electron one (Figure 8(b)) presents two defined regions. The fraction of the white constituent is estimated to be around 12.3%. According to Skeist [22], zinc oxide constituents are added to the phenolic resin in order to improve its corrosion resistance.

The EDS analysis made on a whole image (Figure 8(c)) shows the presence of iron, which agrees to the resin's color; thus, one can infer that any iron oxide was used as the pigment for this kind of resin.

Moreover, the EDS analysis shows a significant presence of Zn and P within the composition of the white constituent. Their presence can mean a gradient in terms of chemical composition for the whole system, avoiding major variations from one layer to another.

The layer based on MoS_2 composition can be observed in Figure 9, where its surface containing microparticles is uniformly dispersed. This pattern was also described in other investigations [23, 24]. In fact, these microparticles of MoS_2 and Sb_2O_3 are suspended in the solution of the phenolic resin diluted in an organic solvent [19].

Figure 10 shows the 3D surface image of the MoS_2 surface (Figure 10(a)) and the correspondent polar graph with texture directions (Figure 10(b)).

Comparing Figures 10(a) and 8(b), one can affirm that the pattern of topography imposed by the zinc phosphate deposition was not much altered up to the MoS_2 layer. In terms of isotropy (Figure 10(b)), it is worthy to note that the main texture directions are the same as those described for the shot blasting (Figure 4(b)).

These findings can be analyzed by means of a summary of surface roughness results, shown in Figure 11, as well as each effect caused by the different steps of manufacturing.

Considering the average roughness in terms of the Sq parameter, the shot-blasted pattern (Figure 4) was significantly modified by the basecoat deposition, as previously discussed. On the other hand, the deposition of MoS_2 diminished the average roughness. A probable reason for that is because the MoS_2 layer was able to fill the spaces left after the basecoat deposition. If one considers the height distribution, the MoS_2 layer brings back the Gaussian values of Ssk and Sku with relatively low deviations, which supports the previous reasoning.

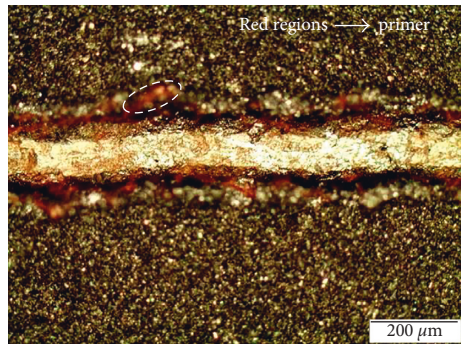

Figure 7: Optical image of a scratched surface of the resin-bonded MoS_2 coating. Red regions represent the basecoat.

Considering the symmetry of surface finishing, significant changes can be described taking into account the Ssk parameter. After the shot-blasting process, although a Gaussian distribution has been described, both zinc phosphate and primer layer depositions increased the skewness. It means that the number of peaks was sufficiently high in comparison to the valleys, and even the average value of heights has been reduced.

4. Conclusions

This investigation presented a detailed analysis of surface changes along the different steps of manufacturing of a three-layer coating applied on AISI 4130 steel. Based on them, the following conclusions can be presented:

(i) The ball-cratering method was successfully used to determine the thickness of the zinc phosphate layer, for single- and multiple-layer systems, using a diluted solution with smaller particles and a preconditioning of the ball.

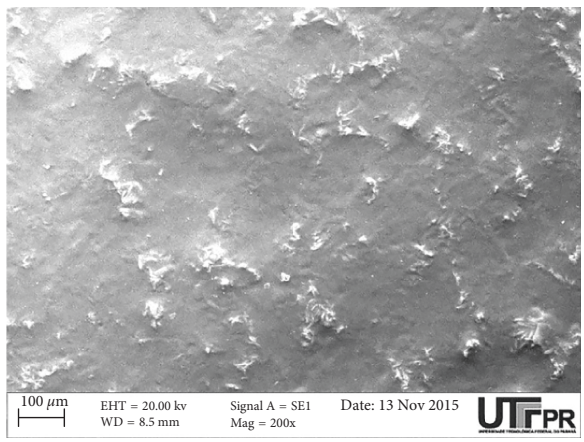

(a)

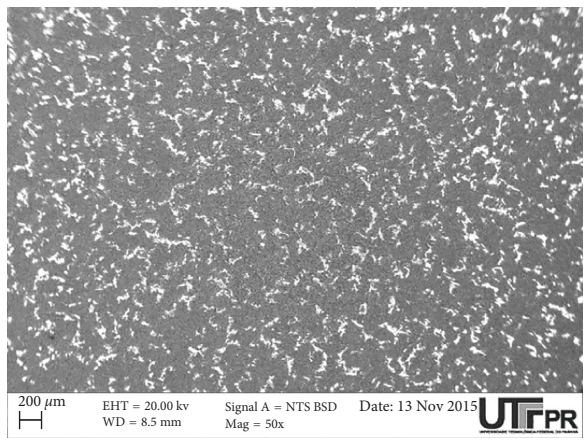

(b)

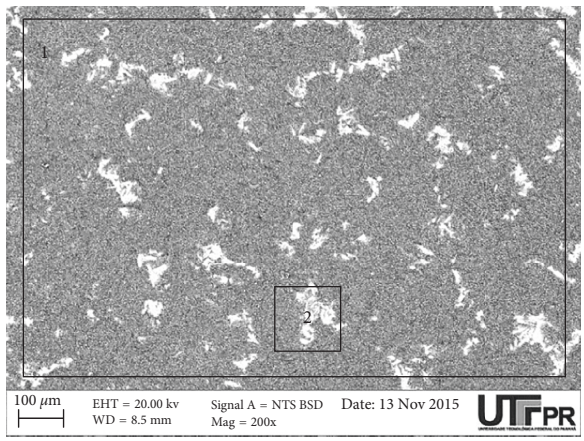

Element weight (%)	C	O	P	Fe	Zn
Region 1 (total area)	71.1	21.2	0.8	5.6	1.3
Region 2 (white particles)	66.3	28.3	2.9	4.2	5.4

(c)

Figure 8: (a) SEM image (SE) of the basecoat surface, (b) SEM image (BSE) of the basecoat surface, and (c) zoom of the SEM image (BSE) with EDS analysis on two regions.

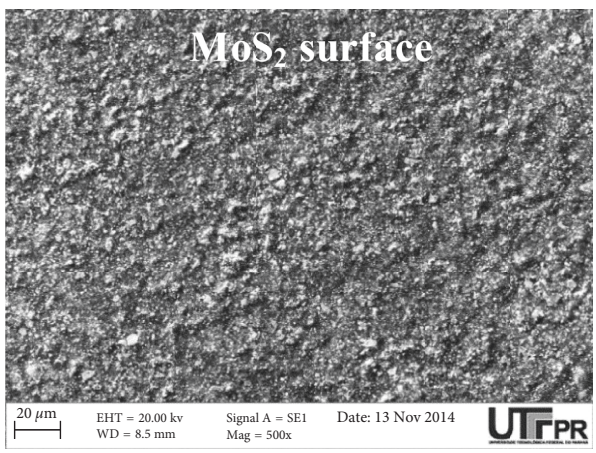

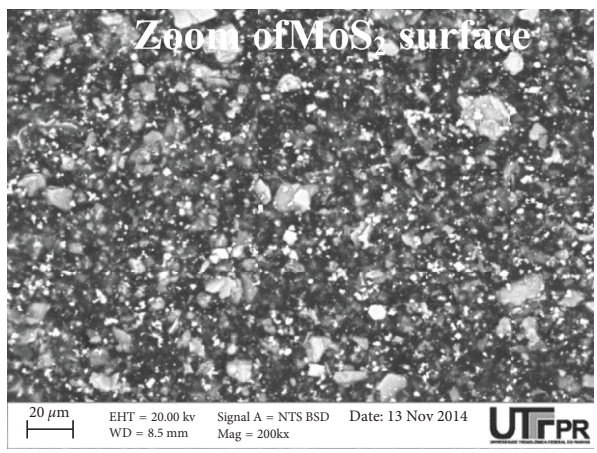

Element	C	O	S	Mo	Sb	Fe
Weight (%)	67.5	16.7	4.1	5.3	6.1	0.2

Figure 9: SEM surface image of the MoS_2 surface (a and b) and EDS analysis of the global surface.

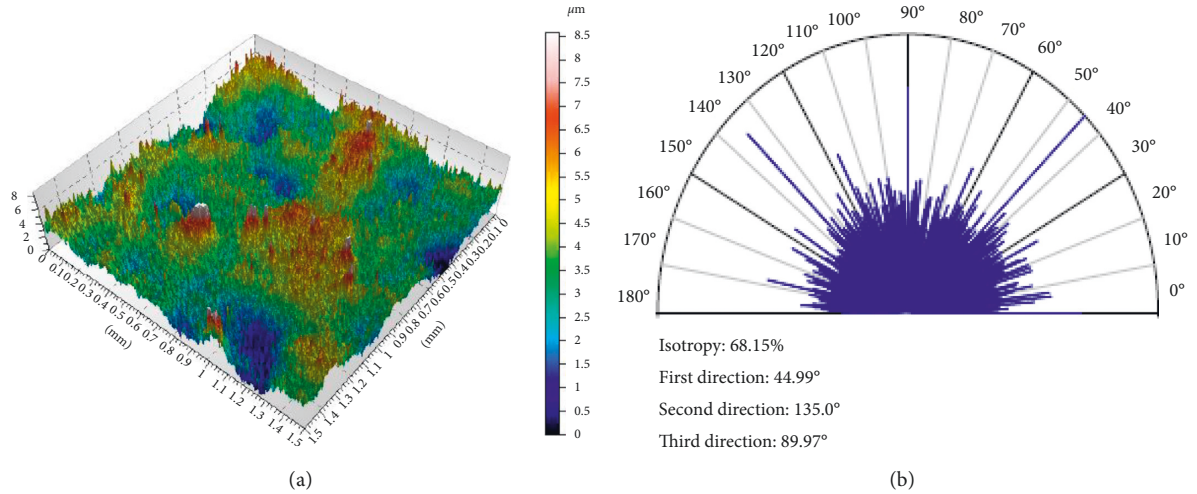

FIGURE 10: (a) 3D surface image of MoS_2 and (b) the polar graph with texture directions.

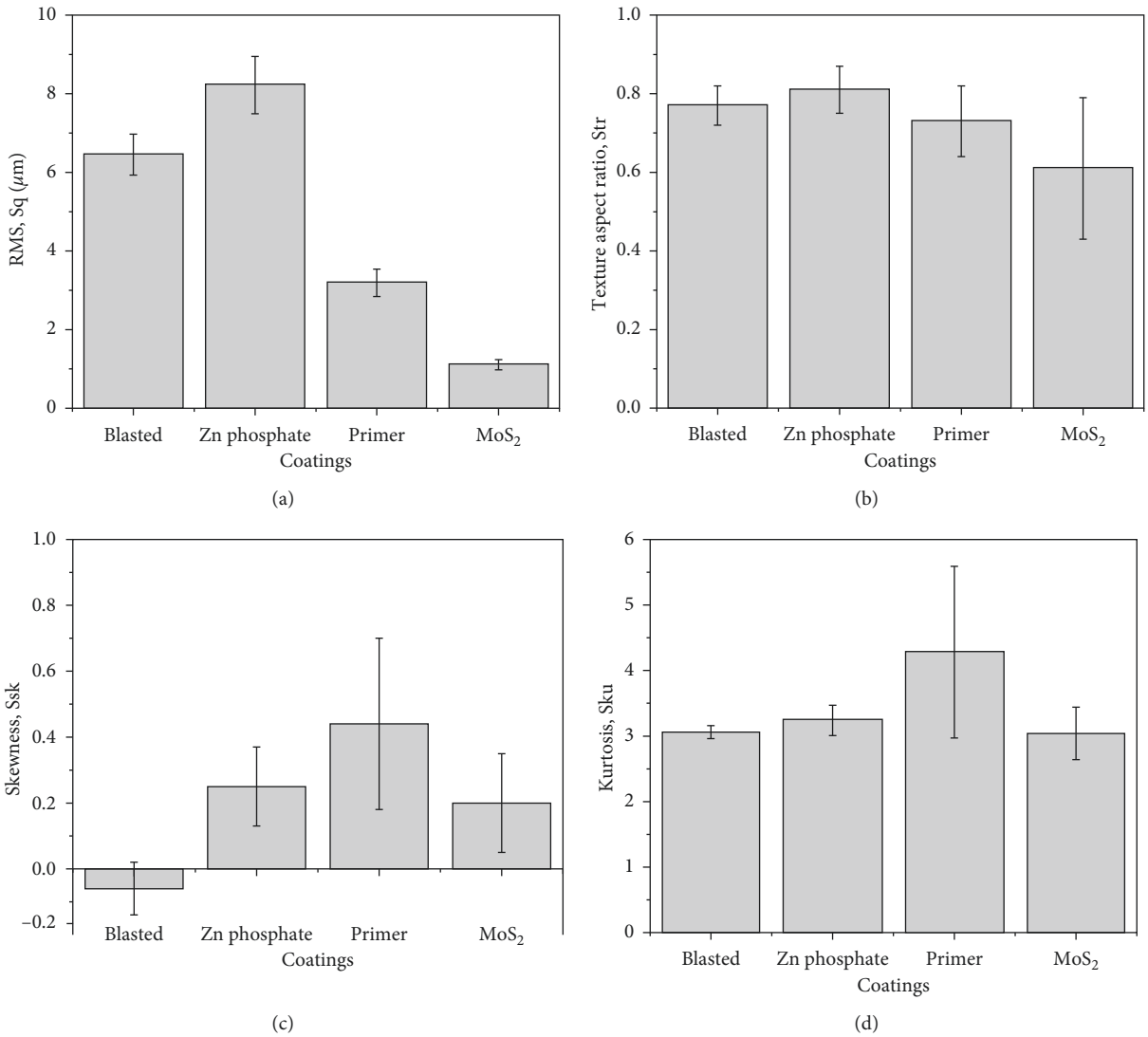

FIGURE 11: Average values of roughness parameters to each step of the layer's deposition: (a) RMS Sq (mm); (b) texture aspect ratio Str; (c) skewness Ssk; and (d) kurtosis Sku.

(ii) For the multiple-layer system, the thicknesses measured by the ball-cratering method were 37% higher than those values determined by SEM, for the basecoat (primer resin) and topcoat (MoS_2 layer).

(iii) Phosphating promotes a significant change in the number of peaks, revealed by the skewness. The surface analysis corroborates the correlation between the surface roughness and phosphating reactions described by Zhang and Kapoor [21].

(iv) The surface isotropy is kept practically the same along all manufacturing processes, meaning that the shot blasting imposed the final texture for that. Besides, few alterations observed in the Str parameter along the manufacturing processes corroborate this observation.

Conflicts of Interest

The authors declare that they have no conflicts of interest.

Acknowledgments

The authors thank CMCM–UTFPR for the facilities in the characterization of materials. Ane C. Rovani thank CAPES for her scholarship. Giuseppe Pintaude acknowledges CNPq for the grant through Project no. 312385/2014-5.

References

[1] J. M. Cunningham, I. J. Ford, J. A. Ogilw, and E. W. Roberts, "Interpretation of friction and wear properties of MoS_2 coated steel substrates," *Wear*, vol. 177, no. 1, pp. 93–101, 1994.

[2] J. H. W. Siu and L. K. Y. Li, "An investigation of the effect of surface roughness and coating thickness on the friction and wear behaviour of a commercial MoS_2–metal coating on AISI 400C steel," *Wear*, vol. 237, no. 2, pp. 283–287, 2000.

[3] K. Wahl, M. Belin, and I. Singer, "A triboscopic investigation of the wear and friction of MoS_2 in a reciprocating sliding contact," *Wear*, vol. 214, no. 2, pp. 212–220, 1998.

[4] Y. Epshteyn and T. Risdon, "Molybdenum disulfide in lubricant applications–a review," in *Proceedings of the 12 Lubricating Grease Conference*, Bonita Springs, FL, USA, June 2010.

[5] M. Melancon, P. Hunter, S. Hourcade et al., "The effect of four commercially available steel decontamination processes on the performance of external coatings," in *Proceedings of the NACE International-International Corrosion Conference*, San Antonio, TX, USA, June 2014.

[6] A. W. Momber, M. Irmer, and N. Glück, "Investigation into the performance of a dual-layer thin-film organic coating during accelerated low-temperature offshore testing," *Journal of Offshore Mechanics and Arctic Engineering*, vol. 139, no. 4, p. 041402, 2017.

[7] J. F. Lin and Y. Yan Guu, "Factors affecting the tribological performance of three resin bonded solid lubricant films," *Tribology Transactions*, vol. 42, no. 3, pp. 601–609, 1999.

[8] E. Roberts and B. Williams, "The effect of substrate surface roughness on the friction and wear of sputtered MoS_2 films," *Journal of Physics D: Applied Physics*, vol. 25, no. 1A, pp. A65–A70, 1992.

[9] A. C. Rovani, G. Pintaúde, F. Kouketsu, and C. da Silva, "Hardness and characterization of coatings employed in subsea equipments," in *Proceedings of the OTC Brazil Offshore Technology Conference*, Rio de Janeiro, Brasil, 2015.

[10] J. S. Zabinski, M. S. Donleya, and N. McDevittb, "Mechanistic study of the synergism between Sb_2O_3 and MoS_2 lubricant systems using Raman spectroscopy," *Wear*, vol. 165, no. 1, pp. 103–108, 1993.

[11] ISO-26423:2009, *Fine Ceramics (Advanced Ceramics, Advanced Technical Ceramics)-Determination of Coating Thickness by Crater-Grinding Method*, 2009.

[12] N. X. Randall, "Finer particle size allows better coating characterization with the Calotest," *Applications bulletin*, vol. 5, pp. 3–6, 1997, http://lab-nnz.ru/wp-content/uploads/05-Finer-particle-size-allows-better-coating-characterization-with-the-Calotest.pdf.

[13] D. Allsopp, R. Trezona, and I. Hutchings, "The effects of ball surface condition in the micro-scale abrasive wear test," *Tribology Letters*, vol. 5, no. 4, pp. 259–264, 1998.

[14] K. I. Schiffmann, R. Bethke, and N. Kristen, "Analysis of perforating and non-perforating micro-scale abrasion tests on coated substrates," *Surface and Coatings Technology*, vol. 200, no. 7, pp. 2348–2357, 2005.

[15] S. L. Zhang, X. L. Zhang, M. M. Zhang, Q. Ma, and W. W. Li, "Effects of alkaline cleaners and cleaning methods on phosphate coating weight and surface morphology," *Transactions of the IMF*, vol. 88, no. 4, pp. 220–224, 2010.

[16] G. Rivero, L. A. Fasce, S. M. Ceré, and L. B. Manfredi, "Furan resins as replacement of phenolic protective coatings: structural, mechanical and functional characterization," *Progress in Organic Coatings*, vol. 77, no. 1, pp. 247–256, 2014.

[17] W. P. Dong, P. J. Sullivan, and K. J. Stout, "Comprehensive study of parameters for characterising three-dimensional surface topography: IV: parameters for characterising spatial and hybrid properties," *Wear*, vol. 178, no. 1-2, pp. 45–60, 1994.

[18] M. C. M. Farias, C. A. L. Santos, Z. Panossian, and A. Sinatora, "Friction behavior of lubricated zinc phosphate coatings," *Wear*, vol. 266, no. 7-8, pp. 873–877, 2009.

[19] S. Rossi, F. Chini, G. Straffelini, P. Bonora, R. Moschini, and A. Stampali, "Corrosion protection properties of electroless nickel/PTFE, phosphate/MoS_2 and bronze/PTFE coatings applied to improve the wear resistance of carbon steel," *Surface and Coatings Technology*, vol. 173, no. 2-3, pp. 235–242, 2003.

[20] E. P. Banczek, P. R. P. Rodrigues, and I. Costa, "Evaluation of porosity and discontinuities in zinc phosphate coating by means of voltametric anodic dissolution (VAD)," *Surface and Coatings Technology*, vol. 203, no. 9, pp. 1213–1219, 2009.

[21] G. M. Zhang and S. G. Kapoor, "The effects of surface roughness on sheet steels after phosphating," *Corrosion Science*, vol. 24, no. 11-12, pp. 977–991, 1984.

[22] I. Skeist, *Handbook of Adhesives*, Chapman & Hall, New York, NY, USA, 1990.

[23] H. J. Song, Z. Z. Zhang, and Z. Z. Luo, "Effects of solid lubricants on friction and wear behaviors of the phenolic coating under different friction conditions," *Surface and Coatings Technology*, vol. 201, no. 6, pp. 2760–2767, 2006.

[24] Z. Xie, Q. Chen, T. Chen, X. Gao, and X. Yu, "Microstructure and properties of nitrogen ion implantation/AlN/CrAlN/MoS_2-phenolic resin duplex coatings on magnesium alloys," *Materials Chemistry and Physics*, vol. 160, pp. 212–220, 2015.